Contribution from Chemistry Department A, The Technical University of Denmark, DK-2800 Lyngby, Denmark, and Laboratoire des Systemès Energêtiques et Transferts Thermiques, associe au CNRS, Universitê de Provence, Centre de St.-Jêrôme, F-13397 Marseille Cedex 13, France

Conductivity, Thermal Analysis, and Phase Diagram of the System $Cs_2S_2O_7$–V_2O_5. Spectroscopic Characterization of $Cs_4(VO_2)_2(SO_4)_2S_2O_7$

G. E. Folkmann,[1a] G. Hatem,[1b] R. Fehrmann,*[,1a] M. Gaune-Escard,[1b] and N. J. Bjerrum[1a]

Received February 4, 1991

The specific conductivities of the solid and molten $Cs_2S_2O_7$–V_2O_5 system were measured at 17 different compositions in the composition range $X_{V_2O_5}$ = 0–0.4100 and in the temperature range 300–500 °C. From the marked change of the conductivity, at the phase transition temperatures the liquidus and the temperatures of fusion of the eutectics could be estimated and the phase diagram of the $Cs_2S_2O_7$–V_2O_5 binary system constructed. The melting point of $Cs_2S_2O_7$ was found to be 461 °C. The phase diagram exhibits a local maximum at $X_{V_2O_5}$ = 0.3333 and t = 412 °C corresponding to the formation of a compound with the stoichiometry $2Cs_2S_2O_7$·V_2O_5. Two eutectics were found at $X_{V_2O_5}$ = 0.168 and $X_{V_2O_5}$ = 0.40 with the temperatures of fusion of 344 and 397 °C, respectively. Differential thermal analysis was carried out on six different compositions in the range $X_{V_2O_5}$ = 0–0.4493. The results agreed well with the phase diagram. IR spectroscopic and EDS investigations of a crystalline compound formed by cooling of a melt with the composition $X_{V_2O_5}$ = 0.33 showed that the compound $Cs_4(VO_2)_2(SO_4)_2S_2O_7$ most probably is formed.

Introduction

The catalyst used for the oxidation of SO_2 by air to SO_3 in the sulfuric acid manufacturing process is well described[2] by the molten salt–gas system $M_2S_2O_7/V_2O_5$–$SO_2/O_2/SO_3/N_2$ (M = alkali metal) at 400–600 °C. Most commercial catalysts are based on K and a minor amount of Na as the alkali metals. However, catalysts based on Cs or Rb have a higher catalytic activity especially at lower temperatures (i.e. below about 430 °C).[3-5] This seems to be caused by the higher ability of the larger alkali-metal cations to stabilize vanadium in the +5 oxidation state,[6] thus preventing the precipitation of compounds with vanadium in the +4 oxidation state, which has been suggested[7-9] to be the reason for the deactivation of catalysts below around 430 °C. Recently it has been shown[10] that V(IV) (and V(III)) compounds indeed are formed in $M_2S_2O_7$–V_2O_5 melts during catalysis at the temperature where the deactivation starts and this temperature of precipitation is lowered by increasing the content of larger alkali-metal cations.

In spite of this, very little is known of the fundamental chemistry of the $Cs_2S_2O_7$–V_2O_5 system. The only melting point of $Cs_2S_2O_7$ reported in the literature (as far as we know) is 280 °C,[11] which is far below the melting point of 461 °C found by us in the present work. However, $Cs_2S_2O_7$ was prepared[11] by heating mixtures of Cs_2SO_4 and concentrated sulfuric acid. This method is equivalent to the method of preparation of $K_2S_2O_7$ from $KHSO_4$, and it seems doubtful[12] that this procedure leads to the formation of pure pyrosulfate. The phase diagram of the system has never been published, but the compounds $CsVO_2SO_4$ and $Cs_4(VO_2)_2(SO_4)_2S_2O_7$ have been reported to be formed[13] by reactions between V_2O_5 and $Cs_2S_2O_7$ (made by heating of $CsHSO_4$). The compounds are reported to melt at 512 and 406 °C, respectively. The Cs analogue of the compound $K_3VO_2SO_4S_2O_7$ (previously isolated from the $K_2S_2O_7$–V_2O_5 system[14]) could not be isolated from the $Cs_2S_2O_7$–V_2O_5 system.[13]

Three papers[15-17] have dealt with conductivity measurements on the $M_2S_2O_7$ and the $M_2S_2O_7$–V_2O_5 (M = Na, K, Rb, Cs) systems. However, the $M_2S_2O_7$ used was prepared by heating $MHSO_4$. This may explain the large discrepancy in the reported[15,16] conductivities of $Cs_2S_2O_7$ at 450 °C.

Furthermore, the conductivity seems to reach a maximum[16,17] with the addition of V_2O_5 to $M_2S_2O_7$ (M = K, Rb, Cs). Our previous measurements[18] on the $K_2S_2O_7$–V_2O_5 system and the present investigation of the $Cs_2S_2O_7$–V_2O_5 system disagree completely with this observation. They show no maximum, but a steadily decreasing conductivity in the range 0–50 mol % V_2O_5.

No thermal investigations of the $Cs_2S_2O_7$–V_2O_5 system have been reported in the literature.

Experimental Section

Materials. $Cs_2S_2O_7$ is not commercially available, nor is $Cs_2S_2O_8$. Therefore, $Cs_2S_2O_8$ was precipitated by mixing nearly saturated solutions of $(NH_4)_2S_2O_8$ and CsOH. After recrystallization and drying, $Cs_2S_2O_8$ was decomposed thermally to $Cs_2S_2O_7$ and the purity of the product, with respect to the possible contaminants $(NH_4)_2S_2O_7$, $CsHSO_4$, and Cs_2SO_4, was checked by Raman spectroscopy as described previously.[10] V_2O_5 was from CERAC (Pure (99.9%)). All handling of chemicals took place in a nitrogen- or argon-filled glovebox with a measured water content of about 5 ppm and continuous gas purification by forced recirculation through external molecular sieves. $Cs_2S_2O_7$ was transferred immediately after synthesis to glass ampules, which were sealed until the chemical was used.

Conductivity Measurements. The borosilicate glass cell with gold electrodes used for measuring the conductivity has been described in detail previously.[18] The cell was filled with chemicals in the glovebox. Thereafter it was evacuated and closed by sealing the stem. The composition of the melt was varied by addition of chemicals through a taper joint, after the cell was cut open in the glovebox. The cell was resealed before it was placed in the measuring furnace.

For each composition the conductivity was measured as a function of temperature in the range 300–500 °C. The temperature was lowered in steps of 10 or 20 °C, until the resistance became larger than 1×10^6 Ω due to crystallization. Sometimes it took several days for the subcooled melt to crystallize. Evidence of subcooling followed by partial crystallization was obtained in one experiment by continuously measuring the conductivity for many hours after lowering the temperature. This experiment is outlined in Figure A of the supplementary material. The

(1) (a) Technical University of Denmark. (b) Universitê de Provence.
(2) Topsøe, H. F. A.; Nielsen, A. *Trans. Dan. Acad. Tech. Sci.* **1947**, *1*, 3, 18.
(3) Jiru, P.; Tomkova, D.; Jara, V.; Vankova, V. *Z. Anorg. Allg. Chem.* **1960**, *303*, 121.
(4) Jensen-Holm, H. Thesis, Department of Chemical Engineering, The Technical University of Denmark, 1978.
(5) Doering, F. J.; Berkel, D. A. *J. Catal.* **1987**, *103*, 126.
(6) Tandy, G. H. *J. Appl. Chem.* **1956**, *6*, 68.
(7) Villadsen, J.; Livbjerg, H. *Catal. Rev.—Sci. Eng.* **1978**, *17*, 203.
(8) Boreskov, G. K.; Polyakova, G. M.; Ivanov, A. A.; Mastikhin, V. M. *Dokl. Akad. Nauk SSSR* **1973**, *210*, 626.
(9) Doering, F. J.; Yuen, H. K.; Berger, P. A.; Unland, M. L. *J. Catal.* **1987**, *104*, 186.
(10) Boghosian, S.; Fehrmann, R.; Bjerrum, N. J.; Papatheodorou, G. N. *J. Catal.* **1989**, *119*, 121.
(11) Spitsyn, V. I.; Meerov. M. A. *Zh. Obshch. Khim.* **1952**, *22*, 905.
(12) Fehrmann, R.; Hansen, N. H.; Bjerrum, N. J. *Inorg. Chem.* **1983**, *22*, 4009.
(13) Glazyrin, M. P.; Krasil'nikov, V. N.; Ivakin, A. A. *Russ J. Inorg. Chem. (Engl. Transl.)* **1982**, *27*, 1740.
(14) Glazyrin, M. P.; Krasil'nikov, V. N.; Ivakin, A. A. *Russ. J. Inorg. Chem. (Engl. Transl.)* **1980**, *25*, 1843.
(15) Kostin, L. P.; Shligerskaya, L. G.; Makarevich, N. A. *Izv. Vyssh. Uchebn. Zaved. Khim. Khim. Tekhnol.* **1975**, *18*, 1015.
(16) Krasil'nikov, V. N.; Ivakin, A. A. *Izv. Akad. Nauk SSSR, Neorg. Mater.* **1988**, *24*, 2047; *Inorg. Mater. (Engl. Transl.)* **1989**, *24*, 1757.
(17) Dubinin, V. G.; Illarionov, V. V.; Maslennikov, B. M. *Kinet. Katal.* **1972**, *13*, 454; *Kinet. Catal. (Engl. Transl.)* **1972**, *13*, 403.
(18) Hatem, G.; Fehrmann, R.; Gaune-Escard, M.; Bjerrum, N. J. *J. Phys. Chem.* **1987**, *91*, 195.

0020-1669/91/1330-4057$02.50/0

subcooled state was stable for more than 16 h, after which a decrease in conductivity over a period of 2 h indicated the formation of crystals. Usually the temperature was then raised in steps of 2 °C. This procedure ensured that possible subcooling of the melt would be detected. In this manner, both the subcooled liquid region and the crystallized region were investigated. The measurements are very time consuming—typically weeks were required to measure one composition.

The temperature of the melt was measured by a calibrated chromel–alumel thermocouple placed directly at the capillary tube. The furnace was regulated to within ±0.1 °C. The furnace and its regulation have been described elsewhere.[19]

The conductivity of a given mixture was obtained by measuring the resistance between the electrodes with either a Wheatstone bridge[18] at 2 kHz or for large resistances a Radiometer CDM-83 conductivity meter. The conductivity, κ, is calculated from $\kappa = k/R$, where R is the resistance and k is the cell constant, determined by measuring the resistance of a standard solution of known conductivity as described earlier.[18] Cell constants of around 200 cm^{-1} were obtained.

Thermal Investigations. Differential thermal analysis (DTA) was carried out in a Calvet type microcalorimeter. The hygroscopic samples were sealed in quartz ampules and crystallized as described in the previous section. However, it was usually necessary to reheat the subcooled sample to around 300 °C and maintain the sample at this temperature for up to 10 h before the crystallization took place. The DTA experiments could only be repeated after slow cooling to room temperature in order to crystallize the sample, since fast cooling leads to glass formation. Heating rates were low, i.e. 10 °C/h. This technique is very sensitive and makes it possible to separate thermal effects due to transitions in the sample appearing at close temperatures. The temperature of the calorimeter was registrated by a Pt/Pt–10% Rh thermocouple with an accuracy of ±1 °C. The calorimeter was calibrated with zinc.

EDS Investigations. Crystalline samples obtained by slow cooling of a $Cs_2S_2O_7$–V_2O_5 melt with the composition $X_{V_2O_5} = 0.33$ were analyzed in a 300-kV Philips EM430 transmission electron microscope equipped with an EDX analyzer (EDAX). The samples were crushed and mounted on a carbon film supported by a copper net in the glovebox. The hygroscopic samples were transferred to the microscope in a closed container. The content of water in the evacuated sample compartment of the microscope was less than 10 ppm during the experiment.

Infrared Spectra. The IR spectra were recorded on a Bomem DA3.26 FTIR spectrometer. The samples were ground with dry KBr or CsBr in the glovebox, and the solids were pressed into transparent disks. The disks were stored in a desiccator when not mounted in the evacuated sample compartment of the spectrometer.

General Considerations

Conductometry. The conductivity of ionic melts depends within wide ranges exponentially on the temperature according to the equation

$$\kappa = A_\kappa e^{-E_\kappa/RT}$$

where κ is the conductivity, A_κ is a constant, E_κ is the energy necessary to promote the ionic migration (the so-called activation energy), R is the gas constant, and T is the absolute temperature.

By plotting the logarithm of the conductivity as a function of the inverse temperature, one usually obtains for the liquid and solid states straight lines with different slopes, as especially E_κ changes when the phase changes. In the intermediate liquid + solid region the curve will deviate from these straight lines. Breakpoints on the ($\ln \kappa$, $1/T$) plots will therefore indicate phase-transition temperatures.

Thermal Measurements. The use of a Calvet microcalorimeter for differential thermal analysis demands the replacement of the temperature regulation system by a linear temperature programmer and a well-defined thermal equilibrium of both thermopiles and their content. Modified in this manner,[20] the apparatus gives rise to a stable baseline up to 1200 K at a heating rate of around 10 K/h. This low heating rate compared to that of conventional DTA instruments is necessary due to the large thermal mass of calorimeter. The inconveniently slow heating rate is compensated by the high sensitivity of the detector and the relatively large sample volume, i.e. around 1 cm^3.

(19) Andreasen, H. A.; Bjerrum, N. J.; Foverskov, C. E. *Rev. Sci. Instrum.* **1977**, *48*, 1340.
(20) Fouque, Y.; Gaune-Escard, M.; Szczepaniak, W.; Bogacz, A. *J. Chim. Phys.* **1978**, *75*, 360.

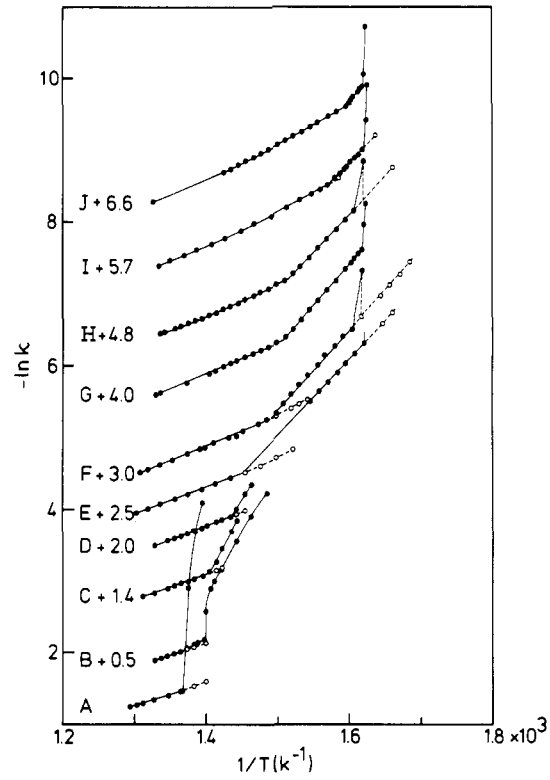

Figure 1. Phase transitions in the $Cs_2S_2O_7$–V_2O_5 system: $-\ln \kappa$ vs $1/T$ for the following compositions. $X_{V_2O_5}$: A, 0.0000; B, 0.0309; C, 0.0542; D, 0.0794; E, 0.0998; F, 0.1149; G, 0.1225; H, 0.1306; I, 0.1496; J, 0.1601. For clarity, the data (except for the those of the pure melt) are offset on the ordinate by the specified values. Open circles indicate subcooling.

EDS Investigations. In order to make possible a quantitative determination, i.e. determination of the relative content of the elements present, the Cliff–Lorimer factors (k factors) were obtained from measurements on known standards. The standards chosen were Cs_2SO_4 (Merck, pro analysis (99.5%)) and $CsV(SO_4)_2$ obtained as earlier described.[10] The standard deviation of the method is around 5%.

Results and Discussion

Conductivity Measurements. The conductivity of the $Cs_2S_2O_7$–V_2O_5 system has been measured at 17 different compositions in the mole fraction range $X_{V_2O_5}$ = 0–0.4100. The highest measuring temperature was 500 °C while the lowest temperature was dependent on the onset of crystallization—the minimum value being around 300 °C. All measured values of the conductivity for each of the compositions investigated are given in the order they were measured in Table A of the supplementary material. The results of the measurements are also shown in Figures 1 and 2, where the specific conductivity, κ, is plotted as $-\ln \kappa$ vs $1/T$. For all compositions, a linear or weakly curved plot is found in the high-temperature region representing the liquid state of the mixture. When melts A–D (Figure 1), corresponding to the compositions $X_{V_2O_5} = 0.0000$ (pure $Cs_2S_2O_7$) and $X_{V_2O_5} = 0.0794$, respectively, are cooled, the conductivity suddenly jumps to a lower value, most probably due to the formation of crystals in the subcooled liquid. When the partly crystallized melt is reheated, the conductivity increases until it coincides with the conductivity curve of the liquid melt at the liquidus temperature of the binary mixture. For the compositions $X_{V_2O_5} = 0.0998$ (E) to $X_{V_2O_5} = 0.1601$ (J) another marked change in the conductivity is found at low temperature. The conductivity becomes undetectably small, i.e. lower than 0.01 μS, below this second breakpoint, indicating that the mixture in the cell is completely crystallized. The breakpoint at the higher temperature for compositions A–J decreases with increasing content of V_2O_5, corresponding to a lowering of the liquidus temperature from 460 °C (A, pure $Cs_2S_2O_7$) to 351 °C (J, $X_{V_2O_5} = 0.1601$). The temperature of the second

Table I. Differential Thermal Analysis on the $Cs_2S_2O_7$–V_2O_5 System: Temperatures[a] of Transitions

sample no.	$X_{V_2O_5}$ (mole fracn)	t, °C: solid-phase transn 1	t, °C: solid-phase transn 2	t, °C: fusion of eutectic 1[c]	t, °C: fusion of eutectic 2[d]	liquidus temp, °C: DTA	liquidus temp, °C: Figure 3
1	0.0000	*b*	*b*			435[e] 462	460
2	0.1998	330		~350		368	366
3	0.2700	328		~347		415	397
4	0.3492		373		~400	420	410
5	0.4084		378		~392	412	402
6	0.4493		370		401	426	437

[a] Average of several measurements. The values marked with ~ are estimates due to overlapping thermal effects. [b] In $Cs_2S_2O_7$ two low-temperature transitions were found at 195 and 292 °C, respectively. [c] Composition of eutectic 1: $X_{V_2O_5} = 0.165$. [d] Composition of eutectic 2: $X_{V_2O_5} = 0.40$. [e] Premelting temperature.

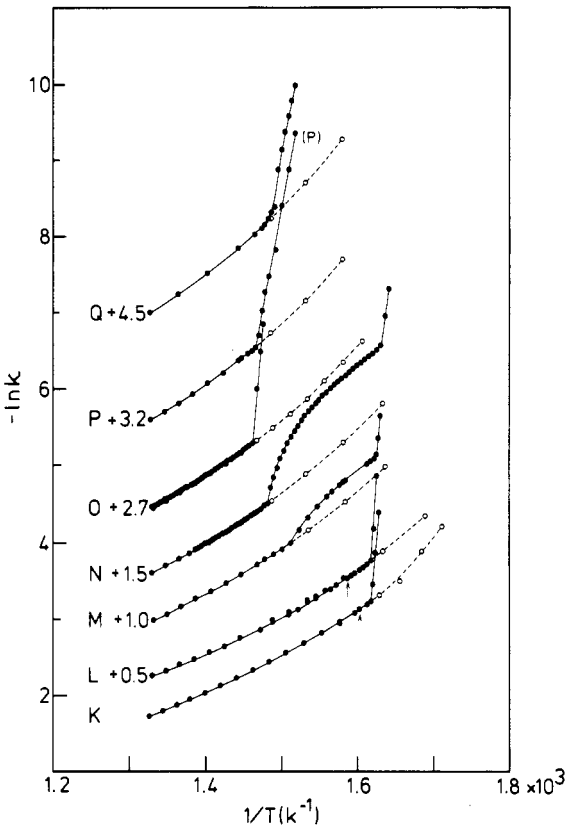

Figure 2. Phase transitions in the $Cs_2S_2O_7$–V_2O_5 system: $-\ln \kappa$ vs $1/T$ for the following compositions. $X_{V_2O_5}$: K, 0.1749; L, 0.1840; M, 0.2534; N, 0.2899; O, 0.3332; P, 0.3747; Q, 0.4100. For clarity, the data (except those for composition K) are offset on the ordinate by the specified values. Open circles indicate subcooling.

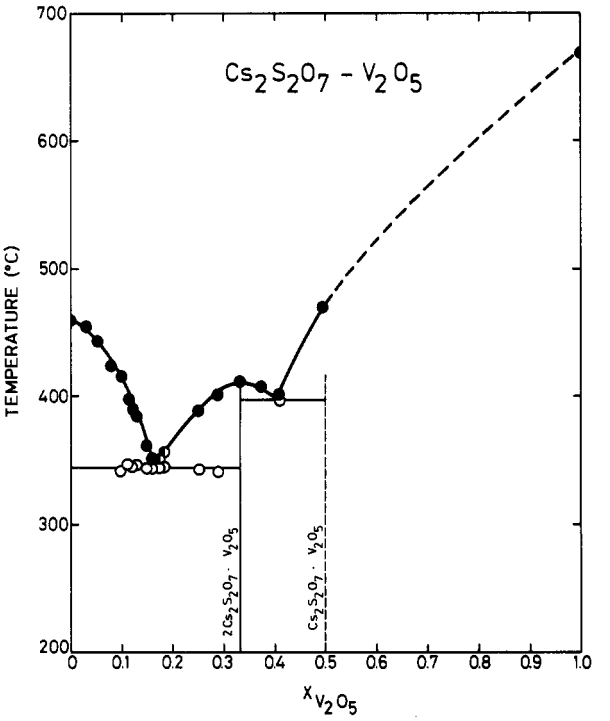

Figure 3. Phase diagram of the $Cs_2S_2O_7$–V_2O_5 system obtained from the conductance measurements. Open circles indicate the melting point of a eutectic phase. Half-filled circles indicate maximum for the liquidus temperatures. The solid-phase transition temperatures, obtained by DTA and given in Table I, are omitted. The dashed line indicates less evidence of the existence of the compound $Cs_2S_2O_7 \cdot V_2O_5$.

breakpoint (the temperature of fusion of the eutectic) is, within experimental error, 344 °C, independent of compositions F–J. The dashed vertical lines on the plot of melts E, F, and H indicate the lower limit of the temperature of the second breakpoint. The liquidus and the fusion temperature of the eutectic for compositions A–J are shown as the left branch of the phase diagram in Figure 3. It should be noted that—as expected—the temperature regime between the two breakpoints, i.e. the liquidus and the temperature of fusion of the eutectic, where a mixture of solid and liquid is present, becomes increasingly smaller as the composition approaches the low-melting eutectic mixture. For the mixtures with $X_{V_2O_5} = 0.1749$ (K) to $X_{V_2O_5} = 0.4100$ (Q) (Figure 2), the breakpoint corresponding to the liquidus temperature increases up to the composition $X_{V_2O_5} = 0.3332$ (O), followed by a decrease in going to $X_{V_2O_5} = 0.4100$ (Q). For compositions K and L, which are close to the eutectic composition $X_{V_2O_5} = 0.168$, the temperature region between the liquidus and the fusion of the eutectic is expected to be small, and subcooling is difficult to detect. Furthermore, during cooling, the temperature was lowered in rather large steps, i.e. 10–20 °C, making detection of the liquidus temperature uncertain. However, the maximum for the liquidus temperature, indicated by an arrow in Figure 2, could be found as the temperature where the conductivity measured during reheating coincides with the conductivity measured during cooling of the sample. These liquidus temperatures are given as half-filled circles in Figure 3. The plot of these data in Figure 3 shows a local maximum of the liquidus temperature of 412 °C at $X_{V_2O_5} = 0.3333$. For compositions K–N, a second break could be observed at the temperature of fusion of the eutectic mixture with the composition $X_{V_2O_5} = 0.168$. For the composition $X_{V_2O_5} = 0.4100$, a second break is observed at 397 °C, probably corresponding to the temperature of fusion of the second eutectic mixture found around $X_{V_2O_5} = 0.40$. The liquidus point at 470 °C for $X_{V_2O_5} = 0.49$ is found by calorimetric measurements of the heat of mixing for the system $Cs_2S_2O_7$–V_2O_5.[21] Finally, the right branch of the phase diagram (dashed curve) extrapolates to 670 °C—the temperature of fusion of V_2O_5.

Thermal Measurements. Six different compositions of the $Cs_2S_2O_7$–V_2O_5 system contained in sealed quartz ampules were examined by differential thermal analysis (DTA) in the Calvet microcalorimeter. The crystallized samples were run several times in the temperature range 300–500 °C. The thermograms are

(21) Folkmann, G. E.; Hatem, G.; Fehrmann, R.; Gaune-Escard, M.; Bjerrum, N. J. To be submitted for publication.

shown in Figure B of the supplementary material. The results are summarized in Table I. The phase-transition temperatures found by DTA are in good accord with the phase diagram in Figure 3. Furthermore, temperatures of solid–solid transitions are observed by the DTA method. However, the phase-transition temperatures found by DTA are generally somewhat higher than those found by conductometry, possibly due to the dynamic nature of the DTA measurements. The melting point of $Cs_2S_2O_7$ is found to be 462 °C by DTA. It compares well with the value of 460 °C found from the conductivity measurements. The melting point of $Cs_2S_2O_7$ can then—as an average—be given as 461 °C.

Compound Formation in the $Cs_2S_2O_7$–V_2O_5 System and Spectroscopic Characterization. In the phase diagram (Figure 3) the vertical lines at $X_{V_2O_5}$ = 0.3333 and 0.5000 indicate the stoichiometric compositions $2Cs_2S_2O_7 \cdot V_2O_5$ and $Cs_2S_2O_7 \cdot V_2O_5$, corresponding to the compounds $Cs_4(VO_2)_2(SO_4)_2S_2O_7$ and $CsVO_2SO_4$, reported[13] to be isolated from the $Cs_2S_2O_7$–V_2O_5 system. The maximum found in the phase diagram at $X_{V_2O_5}$ = 0.3333 points indeed to the existence of a compound with the composition $2Cs_2S_2O_7 \cdot V_2O_5$. This compound might be formulated as $Cs_4(VO_2)_2(SO_4)_2S_2O_7$—the dimeric cesium analogue of the potassium compound $K_4(VO_2)_2(SO_4)_2S_2O_7$, whose existence had been claimed earlier.[14] The melting point of the cesium compound, $Cs_4(VO_2)_2(SO_4)_2S_2O_7$, was found[13] to be 406 °C, which compares well with the phase diagram where the liquidus temperature is found to be 412 °C at $X_{V_2O_5}$ = 0.3333. The compound $Cs_2S_2O_7 \cdot V_2O_5$ might be formed at $X_{V_2O_5}$ = 0.5. It might possibly[13] be formulated as $CsVO_2SO_4$, as similarly suggested[14] for its potassium analogue, KVO_2SO_4. The melting point of this compound was found previously to be 512 °C, which is somewhat higher than the liquidus temperature of ~470 °C found in the phase diagram at $X_{V_2O_5}$ = 0.5.

If the compound $CsVO_2SO_4$ is formed in the $Cs_2S_2O_7$–V_2O_5 system, a more detailed study on the composition $X_{V_2O_5}$ = ~0.5 would probably reveal a peritectic in the phase diagram.

Attempts are being made to isolate and characterize crystalline compounds from the $Cs_2S_2O_7$–V_2O_5 system. However, the high viscosity and the pronounced tendency to glass formation of the V_2O_5-rich mixtures pose severe experimental problems.

Slow cooling of a melt in a glass ampule with the composition $X_{V_2O_5}$ = 0.33, corresponding to the maximum in the phase diagram, resulted in a microcrystalline sample. This was confirmed by investigations using the scanning electron microscope, where the crystalline nature of the small particles (not larger than a few micrometers) was confirmed by the diffraction pattern. Particles with a size of the order of 0.1 μm were typically single crystals, while particles around 1 μm in size showed polycrystalline diffraction patterns. About 30 particles were investigated, and of these, 25 particles showed very similar Cs:V:S molar ratios. The other particles either did not contain all of the three elements or contained Si (probably due to glass pieces introduced into the sample by the opening of the glass ampule). These particles were not included in the calculation of the Cs:V:S ratio. On the basis of the *k* factors obtained from the standards, the V:S ratio was found to be 1:1.9 (±5.1%) and the Cs:V ratio to be 1.9:1 (±3.7%) for the 25 particles. After 30–60 s of radiation, nearly all of the crystalline particles became amorphous and changed shape, most probably due to the melting of the compound. However, the peak intensities did not change in time during the recording of the X-ray spectra. This indicates that no serious change in the composition of the compound took place, e.g. by evaporation. Taking the possibility of a systematic deviation of the *k* factor estimation of ~5% into account, the Cs:V:S molar ratio might be 2:1:2 within experimental error. This molar ratio is in accord with the proposed formula, $Cs_4(VO_2)_2(SO_4)_2S_2O_7$, for the compound.

The IR spectrum of this yellowish brown compound in a pressed KBr disk (0.7 mg in 100 mg of KBr) is shown in Figure 4 (spectrum B) together with the spectrum of $Cs_2S_2O_7$ (1.3 mg in 200 mg of CsBr). The latter spectrum seems not to have been recorded previously. A spectrum of $Cs_2S_2O_7$ recorded in KBr instead of CsBr showed no change of the spectral features. Tentative assignments of the bands for $Cs_4(VO_2)_2(SO_4)_2S_2O_7$ are given in Table II. There seems to be good agreement between the frequencies observed by us and by Glazyrin et al.[13] It is therefore likely that we are dealing with the same compound although no quantitative analysis of the compound was performed in ref 13. The fundamentals of the free-group vibrations of the complex ions, VO_2^+, SO_4^{2-}, and $S_2O_7^{2-}$, are expected to be shifted somewhat in frequency and degeneracies split, due to the effect from the neighboring ions and the low symmetry within the crystal. Indeed, many bands are found in the regions of stretching vibrations. These regions are usually located[22] around 1000 cm^{-1} (ν_1) and 1100 cm^{-1} (ν_3) for the SO_4^{2-} ion. (The regions for the bending vibrations are usually found around 600 cm^{-1} (ν_4) and

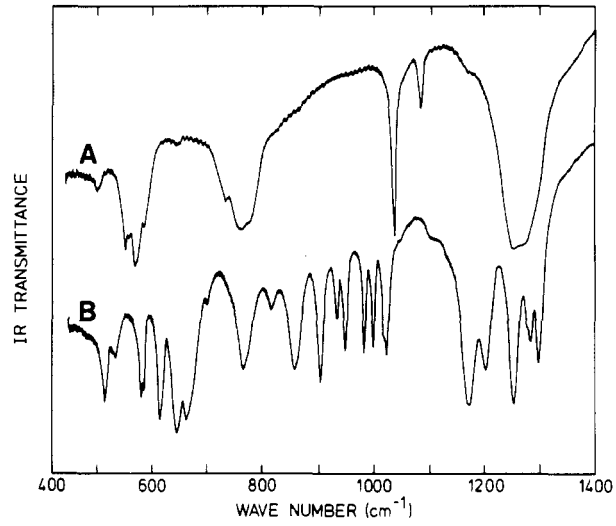

Figure 4. Infrared spectra of $Cs_2S_2O_7$ (A) in CsBr and of the possible compound $Cs_4(VO_2)_2(SO_4)_2S_2O_7$ (B) in KBr. Resolution = ca. 1 cm^{-1}.

Table II. Infrared Bands (cm^{-1}) of $Cs_2S_2O_7$ and the Possible Compound $Cs_4(VO_2)_2(SO_4)_2S_2O_7$ and Their Assignments[a]

	$Cs_4(VO_2)_2(SO_4)_2S_2O_7$		$Cs_2S_2O_7$
	this work	Glazyrin et al.[13]	this work
$\nu(S_2O_7^{2-})$	1297 s	1305	1299 w
	1280 m	1285	1273 s
	1275 w		
	1252 s	1260	1256 s
	1201 m	1210	
$\nu_3(SO_4^{2-})$	1171 s	1180	
	1105 w		1088 m
	1024 s	1035	1040 s
	1018 w		
$\nu_1(SO_4^{2-})$	998 s	1055	
	983 s	990	
	949 s	965	
	934 m	940	
	905 s	915	866 w
$\nu(VO_2^+)_{str}$	861 s	870	823 w
$\nu(S_2O_7^{2-})$	816 m	825	779 m
	768 s	780	766 s
	701 w		739 m
	673 w		
$\nu_4(SO_4^{2-})$	664 s	670	
	646 s	655	
	621 w		
	616 s	620	
$\nu(S_2O_7^{2-})$	587 m		593 m
	583 s	590	574 s
$\nu_2(SO_4^{2-})$	537 w	540	564 w
	517 s	520	557 m
		460	
$\nu(V-L)_{str}$[b]		435	

[a] Key: w, weak; m, medium; s, strong. [b] L is the SO_4^{2-} and $S_2O_7^{2-}$ ligands.

(22) Nakamoto, K. *Infrared and Raman Spectra of Inorganic and Coordination Compounds*; Wiley: New York, 1978.

450 cm^{-1} (ν_2).) This points to a lowering of the T_d symmetry of the SO_4^{2-} ion, possibly due to bidentate coordination, as judged from the number of bands in the range 1000–1300 cm^{-1}.[22] The IR spectrum of $Cs_2S_2O_7$ (spectrum A in Figure 4) exhibits the same features as that of $K_2S_2O_7$, and the frequencies listed in Table II agree very well with the frequencies observed previously[12] for $K_2S_2O_7$. By comparison with spectrum B in Figure 4, strong bands due to $S_2O_7^{2-}$ in the proposed compound, $Cs_4(VO_2)_2(SO_4)_2S_2O_7$, might be located at the highest frequencies, i.e. 1250–1300 cm^{-1}, and around 775 and 575 cm^{-1}. The strong and narrow band found for $Cs_2S_2O_7$ at 1040 cm^{-1} might be the strong band found at 1024 cm^{-1} in spectrum B. It is characteristic that all of the strong bands found for the $S_2O_7^{2-}$ ion in $Cs_2S_2O_7$ are shifted somewhat in frequency and split into more components, probably due to the coordination to the central vanadium atom in the complex compound. The two IR-active stretching modes for the bent VO_2^+ entity are found in the range 1030–875 cm^{-1}, depending on the type of ligands connected to the metal.[23-25] The bending mode of VO_2^+ is found in the range 300–400 cm^{-1}, which is out of the range measured here. The stretching bands for the vanadium–ligand bonds are typically found in the range 400–600 cm^{-1}.[23-25] Due to the very large number of bands found for the $Cs_4(VO_2)_2(SO_4)_2S_2O_7$ compound and the overlapping regions of the free-group vibrations of the complex components, it is—as shown in Table II—not possible to make a definite assignment of the bands to specific groups. However, the IR spectra are in agreement with the proposed formula, $Cs_4(VO_2)_2(SO_4)_2S_2O_7$, for the compound.

Further considerations of the conductivity and complex formation in the molten $Cs_2S_2O_7$–V_2O_5 system will be published[26] when the molar conductivities can be calculated from ongoing density measurements of the molten $Cs_2S_2O_7$–V_2O_5 system.

Acknowledgment. Chresten Traeholt, Laboratory of Applied Physics, The Technical University of Denmark, is gratefully acknowledged for conducting the EDS experiments. Further thanks are due to The Danish Technical Research Council, The Danish Natural Science Research Council, and the Henriksens Foundation, which have supported this investigation.

Registry No. $Cs_2S_2O_7$, 50992-48-8; V_2O_5, 1314-62-1; $Cs_4(VO_2)_2(SO_4)_2S_2O_7$, 84662-69-1.

Supplementary Material Available: Table A, listing all measured specific conductivities and temperatures for each of the investigated compositions of the $Cs_2S_2O_7$–V_2O_5 system, Figure A, outlining the experimental evidence of partial crystallization, and Figure B, showing the thermograms obtained on the $Cs_2S_2O_7$–V_2O_5 system (8 pages). Ordering information is given on any current masthead page.

(23) Weidlein, J.; Dehnicke, K. *Z. Anorg. Allg. Chem.* **1966**, *348*, 278.
(24) Griffith, W. P.; Wicking, T. D. *J. Chem. Soc. A* **1968**, 400.
(25) Pausewang, G.; Dehnicke, K. *Z. Anorg. Allg. Chem.* **1968**, *369*, 265.
(26) Folkmann, G. E.; Hatem, G.; Fehrmann, R.; Gaune-Escard, M.; Bjerrum, N. J. Submitted for publication.

Contribution from Lehrstuhl für Anorganische Chemie I,
Ruhr-Universität, D-4630 Bochum, FRG

Switching the Mechanism of Spin-Exchange Coupling in (μ-Oxo)bis(μ-carboxylato)divanadium(III) Complexes by Protonation of the Oxo Bridge

Petra Knopp and Karl Wieghardt*

Received February 5, 1991

Hydrolysis of $LVCl_3$ in methanol/water (4:1) mixtures with the sodium salts of a variety of carboxylic acids (CF_3COOH, FCH_2CO_2H, $ClCH_2CO_2H$, $BrCH_2CO_2H$, HCO_2H, CH_3COOH, C_6H_5COOH) affords green dinuclear complexes $[L_2V^{III}_2(\mu\text{-O})(\mu\text{-carboxylato})_2]^{2+}$, which have been isolated as solid hexafluorophosphate or iodide salts (L = 1,4,7-trimethyl-1,4,7-triazacyclononane, $C_9H_{21}N_3$). From temperature-dependent magnetic susceptibility measurements it was found that the spins of both vanadium(III) ions (d^2) are fully aligned between 10 and 298 K, indicating very strong intramolecular ferromagnetic coupling. From CH_3CN solutions of these green complexes the pink protonated forms $[L_2V^{III}_2(\mu\text{-OH})(\mu\text{-carboxylato})_2]^{3+}$ are generated by addition of concentrated HBr or $HClO_4$. $[L_2V_2(\mu\text{-OH})(\mu\text{-}C_6H_5CO_2)_2]Br_3$ and $[L_2V_2(\mu\text{-OH})(\mu\text{-}CH_3CO_2)_2](ClO_4)_3\cdot H_2O$ have been isolated as red crystals. The former exhibits intramolecular antiferromagnetic spin-exchange coupling ($H = -2JS_1\cdot S_2$, $S_1 = S_2 = 1$; $J = -36$ cm^{-1}, $g = 1.87$). A model is presented to rationalize the dramatic change of mechanism of the spin-exchange coupling upon protonation of the μ-oxo group.

Introduction

In recent years we and others have studied a series of homodinuclear complexes containing the (μ-oxo)bis(μ-carboxylato)dimetal(III) core where the metal(III) ions are either first-row transition metals (Ti,[1] V,[2] Cr,[3] Mn,[4] Fe[5]) with the d-electron configuration increasing stepwise from d^1 to d^5 or second-row transition metals (Mo,[6] Ru[7]). As nonbridging ligands, hydro-

(1) Bodner, A.; Drücke, S.; Wieghardt, K.; Nuber, B.; Weiss, J. *Angew. Chem., Int. Ed. Engl.* **1990**, *29*, 68.
(2) (a) Wieghardt, K.; Köppen, M.; Nuber, B.; Weiss, J. *J. Chem. Soc., Chem. Commun.* **1986**, 1530. (b) Köppen, M.; Fresen, G.; Wieghardt, K.; Llusar, R. M.; Nuber, B.; Weiss, J. *Inorg. Chem.* **1988**, *27*, 721. (c) Knopp, P.; Wieghardt, K.; Nuber, B.; Weiss, J.; Sheldrick, W. S. *Inorg. Chem.* **1990**, *29*, 363.
(3) Martin, L. L.; Wieghardt, K.; Blondin, G.; Girerd, J. J.; Nuber, B.; Weiss, J. *J. Chem. Soc., Chem. Commun.* **1990**, 1767.
(4) (a) Wieghardt, K.; Bossek, U.; Ventur, D.; Weiss, J. *J. Chem. Soc., Chem. Commun.* **1985**, 347. (b) Bossek, U.; Wieghardt, K.; Nuber, B.; Weiss, J. *Inorg. Chim. Acta* **1989**, *165*, 123. (c) Sheats, J. E.; Czernuszewicz, R. S.; Dismukes, G. C.; Rheingold, A. L.; Petrouleas, V.; Stubbe, J.; Armstrong, W. H.; Beer, R. H.; Lippard, S. J. *J. Am. Chem. Soc.* **1987**, *109*, 1435. (d) Wieghardt, K.; Bossek, U.; Nuber, B.; Weiss, J.; Bonvoisin, J.; Corbella, M.; Vitols, S. E.; Girerd, J. J. *J. Am. Chem. Soc.* **1988**, *110*, 7398. (e) Wieghardt, K. *Angew. Chem., Int. Ed. Engl.* **1989**, *28*, 1153 and references therein. (f) Ménage, S.; Girerd, J. J.; Gleizes, A. *J. Chem. Soc., Chem. Commun.* **1988**, 431. (g) Vincent, J. B.; Folting, K.; Huffman, J. C.; Christou, G. *Biochem. Soc. Trans.* **1988**, *16*, 822.

0020-1669/91/1330-4061$02.50/0